Frontiers in **Bioengineering and Biotechnology**

*CORRESPONDENCE
Bibi Fatemeh Haghiralsadat,
fhaghirosadat@gmail.com
Fatemeh Oroojalian,
f.oroojalian@gmail.com,
Oroojalian.f@gmail.com

†These authors have contributed equally
to this work

RETRACTED: Targeted delivery of 5-fluorouracil, miR-532-3p, and si-KRAS to the colorectal tumor using layer-by-layer liposomes

Maryamsadat Shahidi[1†], Omid Abazari[1†], Parisa Dayati[2], Bibi Fatemeh Haghiralsadat[3]*, Fatemeh Oroojalian[4,5]* and Davood Tofighi[6]

[1]Department of Clinical Biochemistry, School of Medicine, Shahid Sadoughi University of Medical Sciences and Health Services, Yazd, Iran, [2]Department of Clinical Biochemistry, Faculty of Medical Sciences, Tarbiat Modares University, Tehran, Iran, [3]Medical Nanotechnology and Tissue Engineering Research Center, Yazd Reproductive Sciences Institute, Shahid Sadoughi University of Medical Sciences, Yazd, Iran, [4]Department of Advanced Technologies, School of Medicine, North Khorasan University of Medical Sciences, Bojnūrd, Iran, [5]Natural Products and Medicinal Plants Research Center, North Khorasan University of Medical Sciences, Bojnūrd, Iran, [6]Department of Psychology, University of New Mexico, Albuquerque, NM, United States

Co-delivery of siRNA or miRNA with chemotherapeutic drugs into tumor sites is an attractive synergetic strategy for treating colorectal cancer (CRC) due to their complementary mechanisms. In the current work, a liposome nanoparticle (Huang et al., Cancer Metastasis Rev., 2018, 37, 173–187) coated by cationic chitosan (CS) using a controlled layer-by-layer (LbL) process was designed to deliver simultaneous si-KRAS, miRNA-532-3p, and 5-Fluorouracil (5-FU) into CRC cells. The LbL NPs exhibited a spherical structure with an average size of 165.9 nm and effectively protected si-KRAS and miRNA-532-3p against degradation by serum and nucleases. Interestingly, the LbL NPs were successfully entered into cells and efficiently promoted cytotoxicity and suppressed cancer cell migration and invasion. *In vivo*, the LbL NPs reduced tumor growth in SW480-tumor-bearing mice models. In conclusion, these results suggested that the LbL NPs co-loaded with 5-FU and miR-532-3p/si-KRAS might provide a promising potential strategy for inhibiting the malignant phenotypes of CRC cells.

KEYWORDS

colorectal cancer, liposome, MiR-532-3p, si-KRAS, 5-fluorouracil

1 Introduction

Colorectal cancer (CRC) includes 10% of human cancers worldwide, with an estimated 1.9 million new cases and 900,000 death in 2020 (Sung et al., 2021). Over the past decade, studies of CRC treatment have become an enthusiastic area in cancer research (Keum and Giovannucci, 2019). Commonly, the primary treatment of CRC patients entails complete tumor removal, which requires surgical intervention. However, approximately a quarter of

CRC cases are diagnosed at the advanced stages, which results in treatment failure and subsequent CRC-caused deaths (Xie et al., 2020). In some instances, 5-Fluorouracil (5-FU)-based systemic chemotherapy might be started before or after surgical resection as an adjuvant treatment (Vodenkova et al., 2020). Of note, the response rate of CRC patients to 5-FU-based therapy continues to remain low due to chemoresistance development originating from the complicated genetic and epigenetic manner of the tumor cells (Blondy et al., 2020). The CRC occurrence and progression are commonly associated with 35%–45% mutation of oncogenic Kirsten Ras sarcoma viral oncogene homolog (Strand et al., 2019) and nearly 50% loss of p53-suppressor function (Huang et al., 2018). The CRC patients with KRAS and p53 mutations are associated with a higher risk of tumor metastasis and a lower survival rate (Porru et al., 2018; Nakayama and Oshima, 2019). Indeed, inhibiting the KRAS oncogene and simultaneously restoring the p53 tumor suppressor-related pathways may be considered an attractive therapeutic strategy for CRC patients (Ye et al., 2020). Emerging evidence has indicated that these molecules can be regulated using small non-coding RNAs (Gu et al., 2017). MicroRNAs (miRNAs), a group of short non-coding RNAs, modulate gene expression by specifically targeting the $3'$ untranslated regions ($3'$UTR) of messenger RNAs (mRNAs) (Lu and Rothenberg, 2018). MiR-532-3p can act as a sensitizer for chemotherapy in CRC through its activating effects on p53 and subsequent cell apoptosis. Furthermore, miR-532-3p inhibits CRC cell growth, invasion, and the epithelial-mesenchymal transition (EMT) phenotype (Gu et al., 2019).

On the other hand, it has recently been reported that utilizing a siRNA for targeting KRAS oncogene is a unique approach to suppressing KRAS-related signaling and inhibiting tumor growth and development (Strand et al., 2019). Some challenges of systemic delivering naked siRNA and miRNAs include high nucleation degradation and poor cellular entrance, resulting in an inefficient gene silencing (Chen et al., 2015; Xie et al., 2018; Yu et al., 2020). Furthermore, despite the promising potentials of siRNA and miRNA in cancer gene therapy, developing effective delivery and co-delivery systems for tumor sites remains a great challenge.

In the recent decade, layer-by-layer (LbL) nanoparticles have been considered potential non-viral RNA delivery systems due to numerous unique features, including control of size, high loading capacity, and high *in vivo* stability (Zhao et al., 2016; Gupta et al., 2018; Zhao et al., 2018). Duo to their nature, LbL nanoparticles can incorporate therapeutic agents such as inhibitors, drugs, proteins, and RNAs in their multilayers (Men et al., 2020). In the current study, we developed a therapeutic system using LbL nanoparticles to simultaneously deliver 5-FU, si-KRAS, and miR-532-3p to CRC cells to attain the synergy therapeutic effects in CRC treatment. Later, our *in vivo* study revealed that the co-delivery system remarkably suppresses tumor growth in tumor-bearing mice.

2 Materials and methods

2.1 Materials

All reagents and materials utilized in the present work were handled under RNase-free conditions. 5-FU, chitosan (75 kDa, 75–85% degree of deacetylation), 3-(4,5-dimethylthiazol-2-yl)-2,5-diphenyl tetrazolium bromide (MTT), 4',6-diamidino-2-phenylindole (DAPI), polyvinylidene fluoride (PVDF), coumarin-6 (C6; ≥99%), sodium hyaluronate (HA), lipid components including cholesterol (van Noort et al., 2014), hydrogenated soybean phosphatidylcholine (HSPC) and 1,2-dipalmitoyl-sn-glycerol-3-phosphoglycerol (DPPG) were obtained from Sigma-Aldrich. A human SW480 cell line and a mouse colorectal cancer cell line CT-26 was purchased from the National Cell Bank (Pasteur Institute, Iran). Dulbecco's modified Eagle's medium (DMEM), fetal bovine serum (FBS), and penicillin-streptomycin (pen-strep 100X solution) were purchased from the Bioidea company, Iran. Phosphate buffer solution (PBS) was obtained from DNAbiotech company, Iran. All RNA sequences were prepared from Metabion (Germany). All antibodies were bought from Santa Cruz Biotechnologies.

2.2 Preparation of 5-FU loaded liposomes

Previous studies used a conventional thin-film hydration technique to prepare a 100 nm 5-FU loaded liposomes (Zhang et al., 2021). Briefly, the lipid mixture was manufactured by combining HSPC, Chol, and DPPG (7:2:1 M ratio) in 20 ml of chloroform-methanol solvent (2:1 v/v) on shaker for 3 h at 25°C. Thin-layered films were formed after complete chloroform removal using rotary evaporation for 1 h at a constant temperature of 43°C (Heidolph, Germany). Subsequently, the dried lipid thin films were hydrated with the PBS (pH 7.4) solution containing 5-FU under continuous stirring using a magnetic stirrer for 1 h at 60°C on a hot plate. The hydrated film was further sonicated for 5 min at 55°C and vortexed for 2 min. The obtained liposomal suspension was centrifuged at 15,000 rpm for 10 min at room temperature to remove unentrapped 5-FU and other impurities. After filtration (0.22-μm), the purified 5-FU-loaded liposomes were re-suspended in PBS (pH 7.4) for storage. Empty liposomes were produced similarly.

2.3 Preparation of multilayered liposomes

Multilayered liposomes were fabricated through a sequential assembly of CS, miR + siRNA, CS, and HA layers onto the surface of the negatively charged cores. For LbL assembly, 1 volume of 5-

FU loaded liposomes (1 mM) was mixed with 1 volume of CS solution (1 mg/ml, dissolved in 1% acetic acid aqueous solution) on a magnetic stirrer at room temperature for 2 h. Then, ultracentrifugation (50,000 rpm, 4°C for 60 min) was performed to pellet down the nanoparticles. Subsequently, purified CS-coated liposomes were mixed with 10 μM of siKRAS and 10 μM of miR-532-3p (1:1 M ratio) in RNase-free water to load RNAs on the CS-liposomes surface. Another CS layer was also deposited on the surface of nanoparticles. Finally, the obtained nanoparticles were mixed with 1 mg/ml HA dissolved in dibasic sodium phosphate buffer (pH = 7.4, 10 mM). Negatively charged COO^- groups of activated HA were attached to positively charged $NH3^+$ groups of CS. Completed LbL nanoparticles (HA-LbL NPs) were stored in PBS solution at 4°C.

2.4 Characterization of various liposomal formulations

The surface morphology of prepared liposomes was monitored using transmission electron microscopy (TEM, H7600, Hitachi, Japan). The average size, polydispersity index (PDI), and zeta potential of the NPs were determined in each step of the synthesis by dynamic light scattering (DLS) using Zetasizer Nano ZS (Madison, WI) (Oroojalian et al., 2017). Before measurements, the nano-formulations were diluted with distilled water and shaken thoroughly at room temperature.

2.5 Drug content and encapsulation efficiency

Entrapment efficiency and release of 5-FU were evaluated by high-performance liquid chromatography (HPLC, YL9100, South Korea). 5-FU-loaded liposomal nanoparticles were placed into a 50 ml falcon tube and centrifuged (15,000 rpm, 20 min, 4°C) to evaluate the drug encapsulation efficiency and loading content (EE and LC) (Pourpirali et al., 2021). After centrifugation, the unencapsulated 5-FU in the pellet was isolated, and the supernatant was placed into 1.5 ml tubes and centrifuged (15,000 rpm, 20 min, 4°C). The pellet containing 5-FU-loaded liposomes was rinsed with 1 ml HPLC grade water to separate any unencapsulated 5-FU, and the amount of 5-FU was determined using the HPLC technique.

The %EE and %LC were measured using the following formulations (Mirhosseini et al., 2020; Pourpirali et al., 2021; Abtahi et al., 2022):

$$EE(\%) = \text{encapsulated drug (mg)}/\text{Total used drugs (mg)} \times 100;$$

$$LC(\%) = \text{weight of encapsulated drugs}/\text{weight of LBL} - NPs \times 100.$$

Name	Sequence (5′ to 3′)
KRAS	Forward: GCCTGCTGAAAATGACTG
	Reverse: TCCTGTAGGAATCCTCTATTG
GAPDH	Forward: GTCTCCTCTGACTTCAACAGCG
	Reverse: ACCACCCTGTTGCTGTAGCCAA
miR-532-3p	Forward: CCCTCCCACACCCAAGG
	Reverse: CCCAGTAGTCGTTCAGTCCA

2.6 *In vitro* 5-FU release

To evaluate *in vitro* 5-FU release, 50 mg of 5-FU-loaded NPs were incubated in 10 ml PBS buffer solutions containing different acidity (pH 7.4 and pH 4.5) in a shaking incubator at the speed of 100 rpm at 37°C. At various time points (0–80 h), the samples were centrifuged (13,000 rpm) for 10 min, and then 25 μl of the supernatant was harvested and tested to determine the amount of released 5-FU by UV-Vis spectrophotometry at 266 nm.

2.7 RNA encapsulation efficiency

The optimal nitrogen to a phosphate (N/P) ratio of HA-LbL NPs and siRNA + miRNA for complexation was evaluated by gel retardation assay. Briefly, 0.5 μg of RNAs was mixed with varying amounts of prepared LbL formulation to obtain different binding ratios in a total volume of 10 μl in RNase-free water with a pH of 7.4 and gently shaken at 37°C. For evaluating RNA encapsulation efficiency, agarose gel electrophoresis was executed for 1 h at 60 V, and then the RNA migration was graphed using an ultraviolet light gel imaging system.

2.8 RNA protection assay

The RNA protection against RNase A was studied using agarose gel electrophoresis. HA-LbL NPs were exposed to 1 μl RNase A at 37°C (0–24 h), followed by agarose gel electrophoresis.

2.9 The stability of LbL NPs in serum environment

The serum stability of the LbL formulation was monitored after incubating HA-LbL NPs in the FBS solution (1:10 volume ratio) at 37°C under gentle stirring. At time points of 0–72 h, the mean diameter of the HA-LbL NPs was measured by DLS.
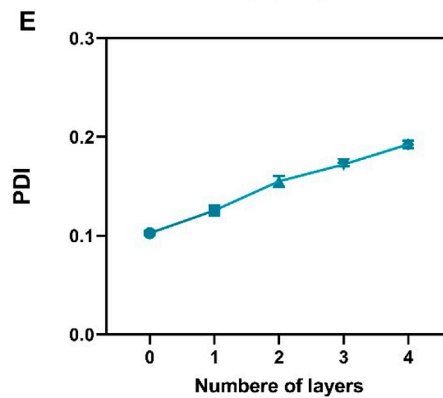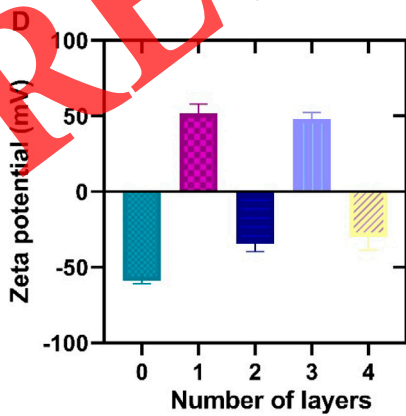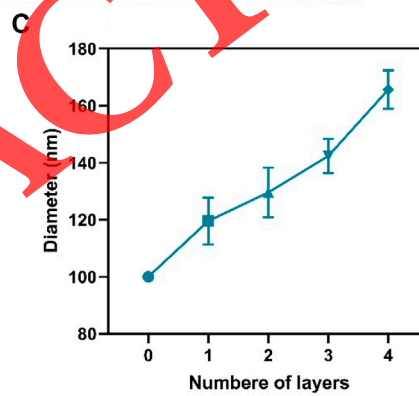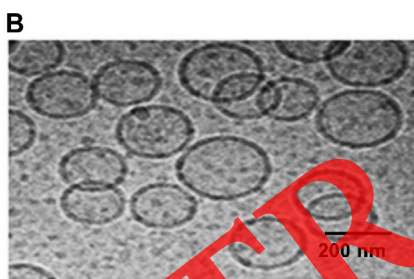
FIGURE 1
(Continued).

FIGURE 1
(Continued). Preparation and physical characterization of HA-LbL NPs. **(A)** Schematic view of the experimental setup; **(B)** The TEM image of Liposome. **(C)** Hydrodynamic diameter, **(D)** zeta potential, and **(E)** PDI of the nanoparticle during HA-LbL preparation. **(F)** The stability of HA-LbL NPs in PBS solution. **(G)** 5-FU release profile from HA-LbL NPs in PBS at different time points (1−80 h). **(H)** Electrophoretic migration of siRNA, miRNA, and HA-LbL NPs. The lane numbers were the mass ratios of LbL NPs/RNAs. **(I)** Agarose gel electrophoretic analysis evaluates the siRNA and miRNA release of HA-LbL NPs at different time points. Data are presented as the mean ± SD. **$p < 0.01$. Abbreviations: PBS, phosphate-buffered saline; LbL NP: layer-by-layer nanoparticle; PDI: polydispersity index; TEM: Transmission electron microscopy; PBS: Phosphate-buffered saline. 0−4 in the Figures 1C−E represent 0: core; 1: chitosan layer; 2: RNA layer; 3: chitosan layer; 4: Hyaluronic acid, respectively.
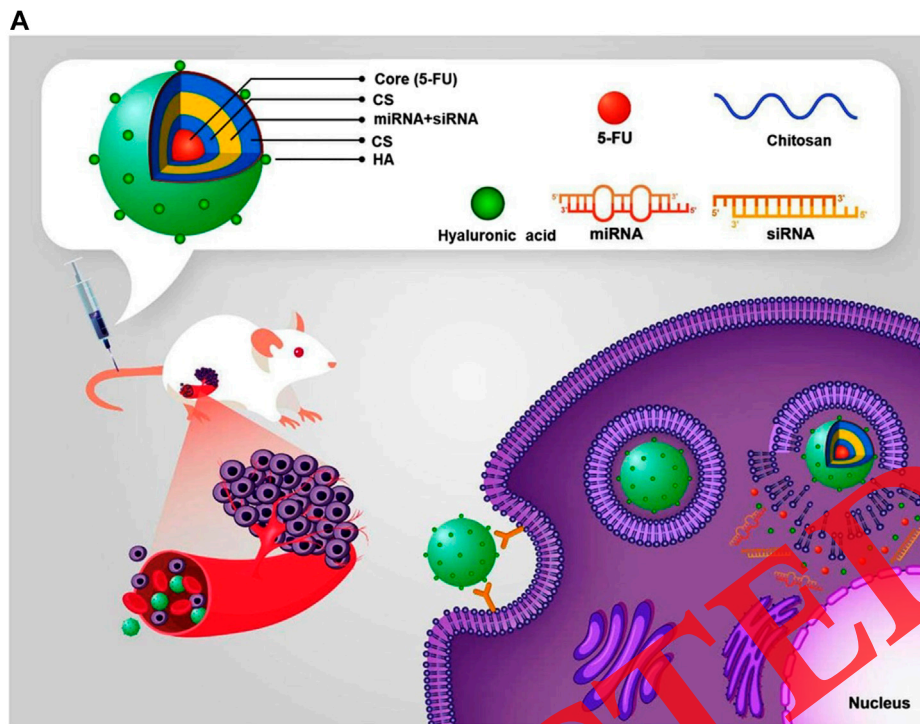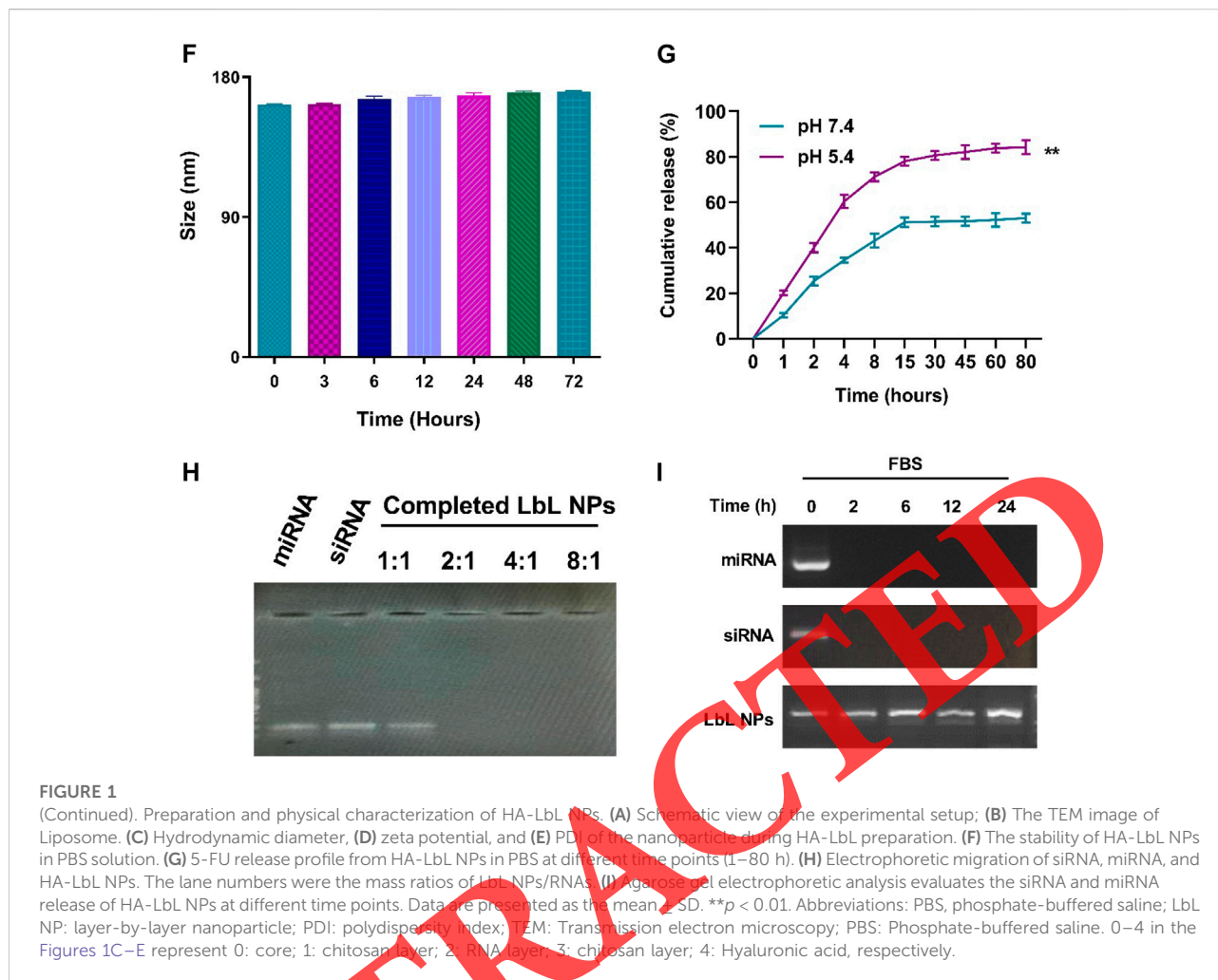
2.10 Blood compatibility

2 ml blood sample containing EDTA was centrifuged for 10 min at 3,000 rpm to monitor the hemolysis rate. Further, various concentrations of HA-LbL NPs were prepared, added to 0.5 ml of 2% red blood cell (RBC) suspension, and incubated for 2 h at 25°C. Then, the mixture was centrifugated for 3 min at 10,000 rpm, and the absorbance of the supernatant was recorded at 570 nm. The negative and positive controls utilized in this experiment were PBS and sterile water, respectively.

$$\text{The hemolysis rate}\,(\%) = (OD1 - OD0)/(OD2 - OD0) \times 100\%$$

OD0, OD1, and OD2 are the values of the negative control, experimental groups, and positive control, respectively.

3 ml of blood containing sodium citrate as an anticoagulant was centrifuged (3,000 rpm, 10 min) to detect the blood clotting indexes, and plasma was isolated. Subsequently, 1 μl PBS and sterile HA-LbL NPs were added to the PBS solution to adjust the

10 μl final volume, which then was mixed with 300 μl plasma and incubated at 37°C for 15 min. Activated partial prothrombin time (APTT), prothrombin time (Gupta et al., 2018), fibrinogen, and thrombin time (TT) were recorded using an automatic blood coagulation instrument.

2.11 Cell culture

The Human SW480 cell line was cultured in DMEM, enriched with 10% FBS, and 1% antibiotic, and kept in an incubator under a standard condition.

2.12 *In vitro* cytotoxicity

The MTT assay was conducted to monitor the *in vitro* cytotoxicity of LbL NPs on the SW480 cell line (Meerloo et al., 2011). In brief, a total of 5×10^4 SW480 cells suspended in a 200 ml culture medium were plated into 96-well plates and
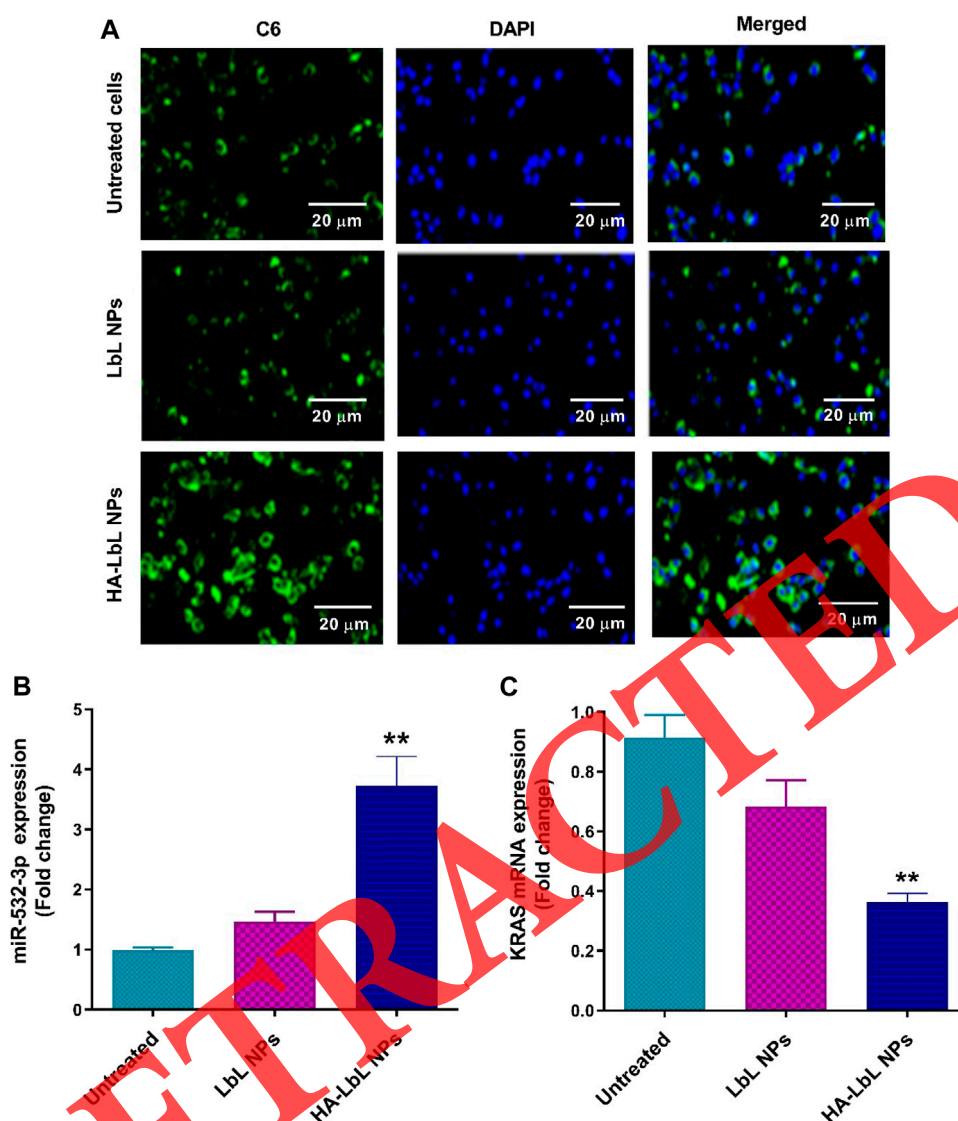
FIGURE 2
Cellular entrance of HA-LbL NPs in SW480 cells. **(A)** Images detected by fluorescence microscopy. Cell nuclei were stained with DAPI (blue). The expression of **(B)** miR-532-3p and **(C)** KRAS after treatment with LbL NPs and HA-LbL N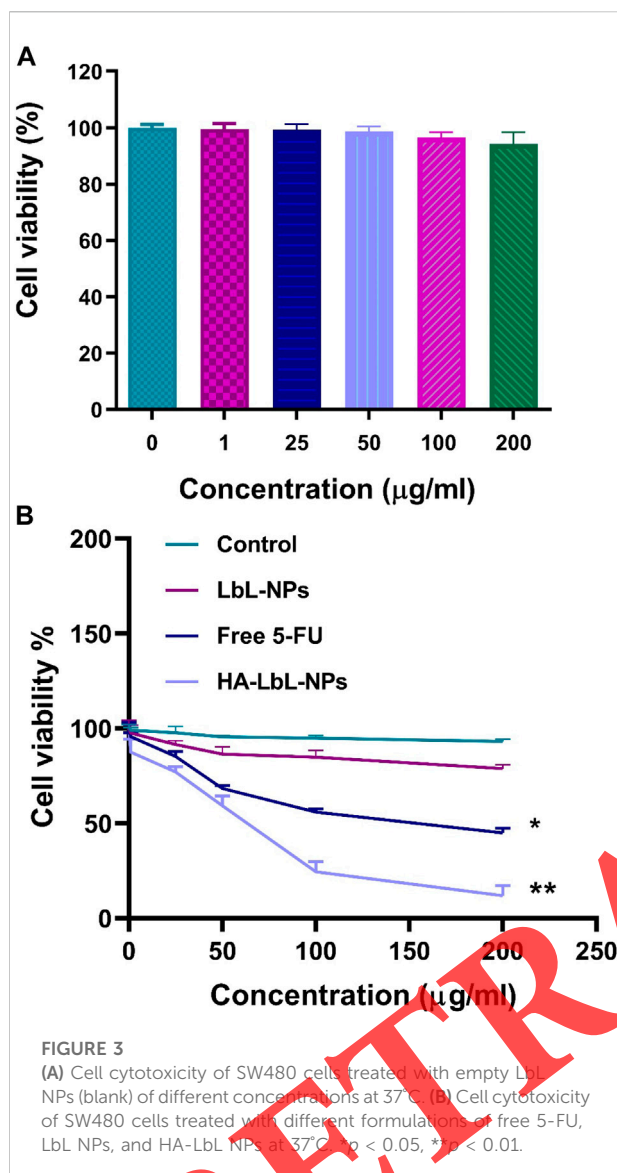Ps. Data are presented as the mean ± SD. **$p <$ 0.01—abbreviations: LbL NP; layer-by-layer nanoparticle; SD: standard deviation.

incubated for 24 h. Further, cells were treated with different concentrations of free 5-FU, LbL NPs, and HA-LbL NPs and incubated for 24 h at 37°C. After incubation, cells were washed twice with PBS and exposed to 200 μl MTT reagent/well (5 mg/ml), and then incubated for an additional 4 h incubation in an incubator (37°C). Then, the culture medium was discarded, 150 μl DMSO was added to each well and shaken for 10 min to dissolve the formazan crystals. The absorbance of each well was recorded at the wavelength of 570 nm using a microplate reader (Bio-Rad, United States). The cell viability was calculated according to following equation:

$$Cell\ viabilit\ y\ (\%) = \frac{OD\ Sample}{OD\ Control} \times 100$$

2.13 Cellular uptake

The cellular uptake rates of LbL NPs and HA-LbL NPs by SW480 cells were visualized by a fluorescence microscope and using coumarin 6 (C6) as a hydrophobic fluorescent molecule. To study the cellular internalization, C6 (20 mg) was incorporated in liposomes for the C6-liposome

FIGURE 3
(A) Cell cytotoxicity of SW480 cells treated with empty LbL NPs (blank) of different concentrations at 37°C. **(B)** Cell cytotoxicity of SW480 cells treated with different formulations of free 5-FU, LbL NPs, and HA-LbL NPs at 37°C. *p < 0.05, **p < 0.01.

formation. Briefly, SW480 cells (1×10^6 cells/well) were cultured in a six-well culture plate containing DMEM supplemented with 10% FBS, and then maintained in the incubator (5% CO_2 and 37°C) overnight. After the cells reached 80–90% confluence, the medium was removed and replaced with a fresh medium containing C6, C6-LbL NPs, and C6-HA-LbL NPs (200 μg/mL). After incubating for 1 h at 37°C, the cells were rinsed three times with cold PBS solution (pH = 7.4) and fixed for 10 min with paraformaldehyde (4%, w/v). Nuclei were stained with DAPI for 15 min (100 μl per well). After being rinsed three times with PBS, the cellular uptake of NPs was observed under a fluorescent microscope (Olympus, Japan).

2.14 Transwell assay

The migration and invasion ability of SW480 cells were determined using the transwell assay. Briefly, SW480 cells at a density of 5×10^4 were suspended in 200 μl of serum-free DMEM, added into upper Transwell chambers, and incubated at 37°C for 24 h. The lower chambers were filled with 600 μL DMEM containing 20% FBS. Next, free 5-FU and HA-LbL NPs solutions were then added to the upper chamber of the Transwell. Following 24 h of incubation, the upper chamber was removed and SW480 cells were fixed with 4% paraformaldehyde for 3 min. After removing the fixation liquid, the cells were stained with 0.1% crystal violet solution for 20 min. Five fields of the cells were randomly counted in under a light microscope.
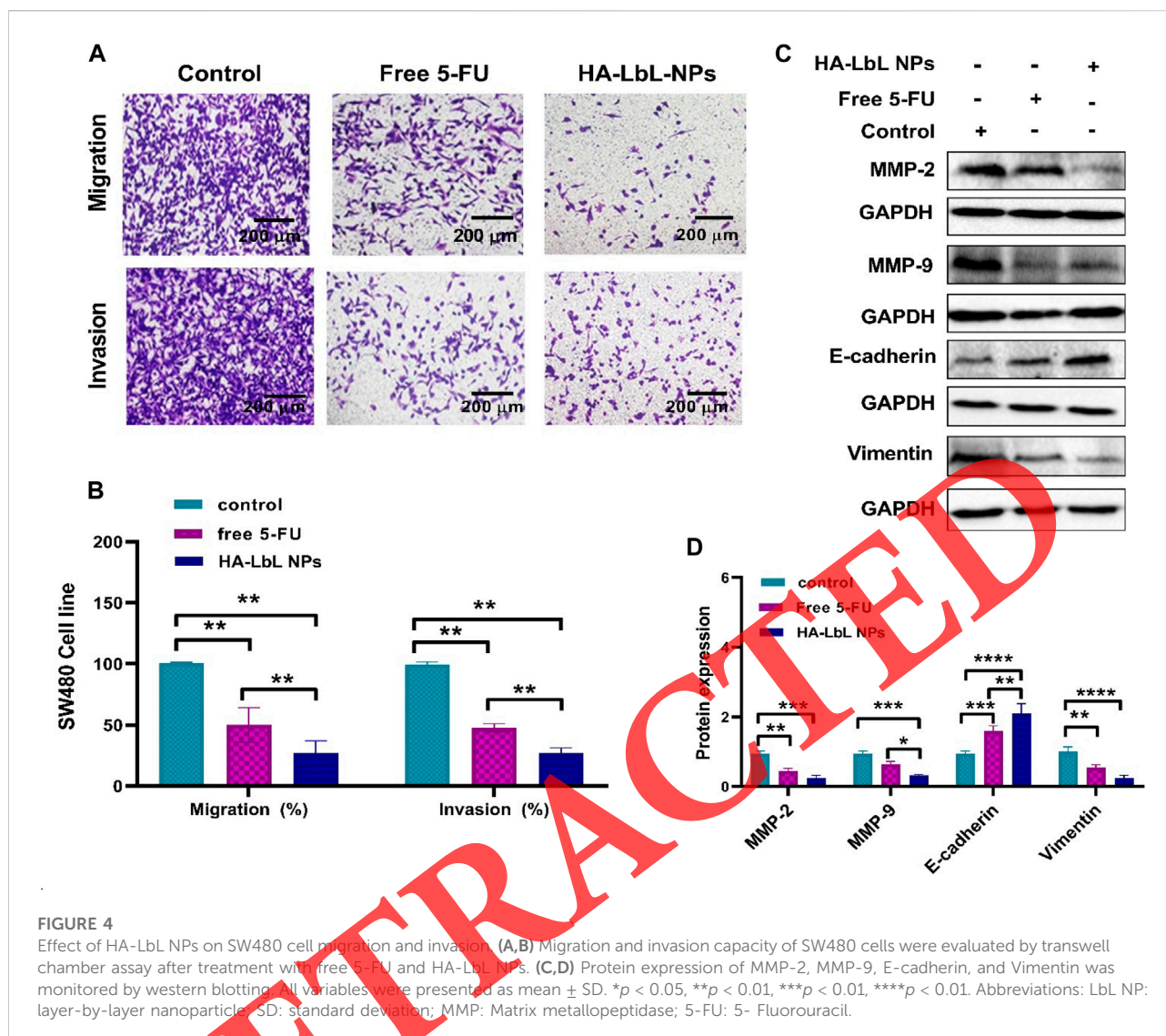
$$\text{The migrated or invaded cells (\%)} = \frac{\text{The number of treated cells}}{\text{The number of control cells}} \times 100$$

2.15 RNA extraction and quantitative real-time PCR

After harvesting treated cell and tissue samples, the Trizol reagent (GENEALL, Korea) was supplied to extract the total RNAs, including miRNA, following the instruction. 1 μg of obtained RNAs was reversed and transcribed using a suitable cDNA synthesis kit (TAKARA, Japan). qPCR amplification was performed using selected primers, SYBR Premix Ex Taq II Kit (TAKARA, Japan), and cDNA template on the ABI-7500 Fast Real-Time System following construction. Relative expression was determined using the $2^{-\Delta\Delta CT}$ method. U6 snRNA and glyceraldehyde 3-phosphate dehydrogenase (GAPDH) were employed to data normalization expression, respectively. The sequence of U6 (600750) as an internal reference for miR-532-3p was from Qiagen (Germany). Sequences of KRAS, miR-532-3P, and GAPDH are listed in Table 1.

2.16 Western blotting assay

Briefly, untreated (control) and treated (free 5-FU and HA-LbL NPs) were harvested, lysed, and then centrifuged for 10 min at 14,000 rpm at 4°C. The supernatant was collected and the total extracted proteins were quantitated by the Bradford assay. Then, 30 μg of each protein sample was run and isolated on 10% sodium dodecyl sulfate-polyacrylamide gel electrophoresis (SDS-PAGE), and the protein bands were absorbed on the PVDF membrane. After blocking with non-fat milk (5%), the membranes were exposed to primary antibodies against

FIGURE 4
Effect of HA-LbL NPs on SW480 cell migration and invasion. **(A,B)** Migration and invasion capacity of SW480 cells were evaluated by transwell chamber assay after treatment with free 5-FU and HA-LbL NPs. **(C,D)** Protein expression of MMP-2, MMP-9, E-cadherin, and Vimentin was monitored by western blotting. All variables were presented as mean $\pm$ SD. $*p < 0.05$, $**p < 0.01$, $***p < 0.01$, $****p < 0.01$. Abbreviations: LbL NP: layer-by-layer nanoparticle; SD: standard deviation; MMP: Matrix metallopeptidase; 5-FU: 5- Fluorouracil.

Vimentin (1: 2000), E-cadherin (1: 2000), matrix metalloproteinase (MMP)-2 (1: 2000), MMP-9 (1: 2000), and GAPDH (internal control; 1: 2000) overnight at 4°C with gentle shaking. After three times washing with TBST (Tris-buffered saline, 0.1% Tween 20) buffer, the membrane was incubated with an appropriate secondary HRP-conjugated antibody for 1 h at room temperature with gentle shaking. The protein signals were detected using enhanced chemiluminescence (ECL) and analyzed by Image J software.
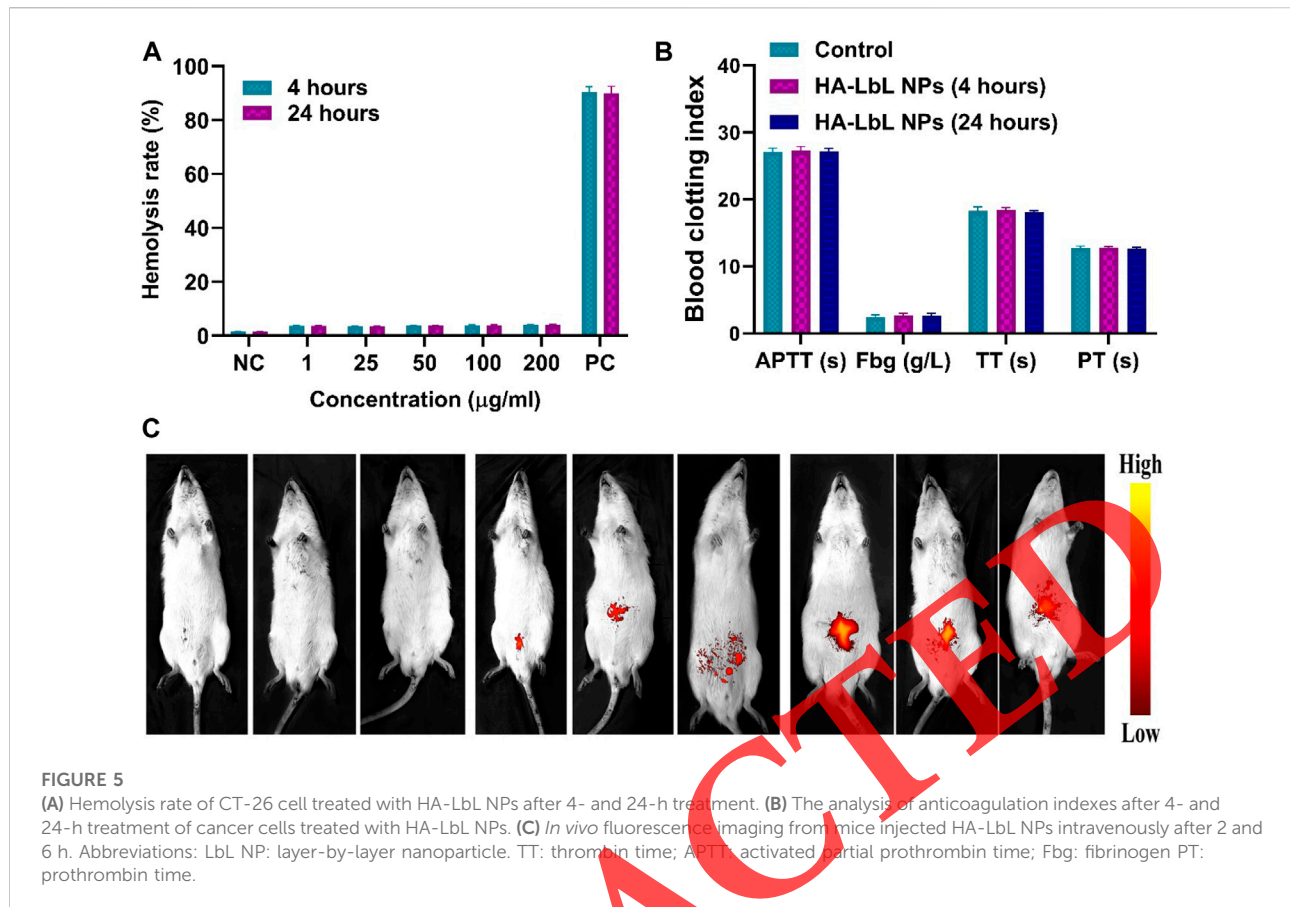
2.17 *In vivo* anti-tumor efficacy

BALB/c mice (4–6 weeks old, 18–25 gr) were purchased from the Shahid Sadoughi University of Medical Sciences (Yazad, Iran) and maintained under specific pathogen-free conditions.

All procedures were supplied following the ethical standards and the care of animal guidelines and approved by the Ethics Committee of Biotechnology research center, Biotechnology research center, International campus, Shahid Sadoughi University of Medical Sciences. CT-26 cells (3×10^5 per 200 µl PBS) were subcutaneously implanted into the right flank region of mice. The tumor growth was checked and measured every 3 days, and the tumor volumes were calculated using the formulation:

$$\text{Tumor volume } (mm^3) = 1/2 \times (\text{length}) \times (\text{width})^2$$

Then, the mice were randomly distributed into three groups (n = 5/each group) and received PBS, 5-FU (100 µl), and HA-liposomal 5FU (100 µl), respectively. The concentration of 5-FU and RNAs was 5 mg/kg and 1 mg/kg, respectively. At 21 days post-injection, all mice were anesthetized using ketamine

FIGURE 5
(A) Hemolysis rate of CT-26 cell treated with HA-LbL NPs after 4- and 24-h treatment. **(B)** The analysis of anticoagulation indexes after 4- and 24-h treatment of cancer cells treated with HA-LbL NPs. **(C)** *In vivo* fluorescence imaging from mice injected HA-LbL NPs intravenously after 2 and 6 h. Abbreviations: LbL NP: layer-by-layer nanoparticle. TT: thrombin time; APTT: activated partial prothrombin time; Fbg: fibrinogen PT: prothrombin time.

(100 mg kg^{-1}) and xylazine (12 mg kg^{-1}), and the blood samples were withdrawn from the mice and analyzed for hemocompatibility evaluation. Mice were sacrificed and the liver, spleen, and lung tissues as well as tumor tissues were isolated and washed in PBS solution. The liver, spleen, and lung tissues were sectioned (5-μm slice) and fixed in 10% neutral buffered formalin for hematoxylin and eosin (H&E) staining. For tumor tissues immunohistochemical (IHC) staining, tumor issues were embedded in paraffin, sectioned, and stained with anti-KI-67 antibody. IHC and H&E staining was carried out according to the to standard protocols (Boyiddle et al., 2017).

2.18 *In vivo* tissue distribution

To biodistribution analysis, mice were distributed into control (PBS) and HA-LbL NPs groups. In brief, 3 mg/kg of HA-LbL NPs was intravenously injected into the tail of tumor-bearing BALB/c mice (4-week-old) and then fluorescence images were taken at 2 and 6 h after injection using an *in-vivo* imaging system (IVIS). Mice healthy (Control) and.

2.19 Statistical analysis

The experiment results were analyzed using Graph Pad Prism (Version 8, GraphPad Software, San Diego, CA). The data were given from three independent measurements and presented as the mean ± standard deviation (mean ± SD). Statistical analysis between different groups was conducted by Student's *t*-test as well as one-way ANOVA, followed by Tukey's post hoc test. $p < 0.05$ was assumed statistically significant.

3 Results and discussion

3.1 Characterization of nanotherapeutics

For simultaneous effective delivery of siRNA/miRNAs to the target tumor site, it is important to employ suitable carriers for RNAs protection from degradation against serum RNases and regulating RNAs circulation time (Eygeris et al., 2020). In the present work, we employed the LbL approach to improve loading and successful delivery of 5-FU and RNAs to the CRC site. To prepare the HA-LbL NPs, 5-FU was first entrapped in the aqueous core of the liposomal vesicle during thin-film
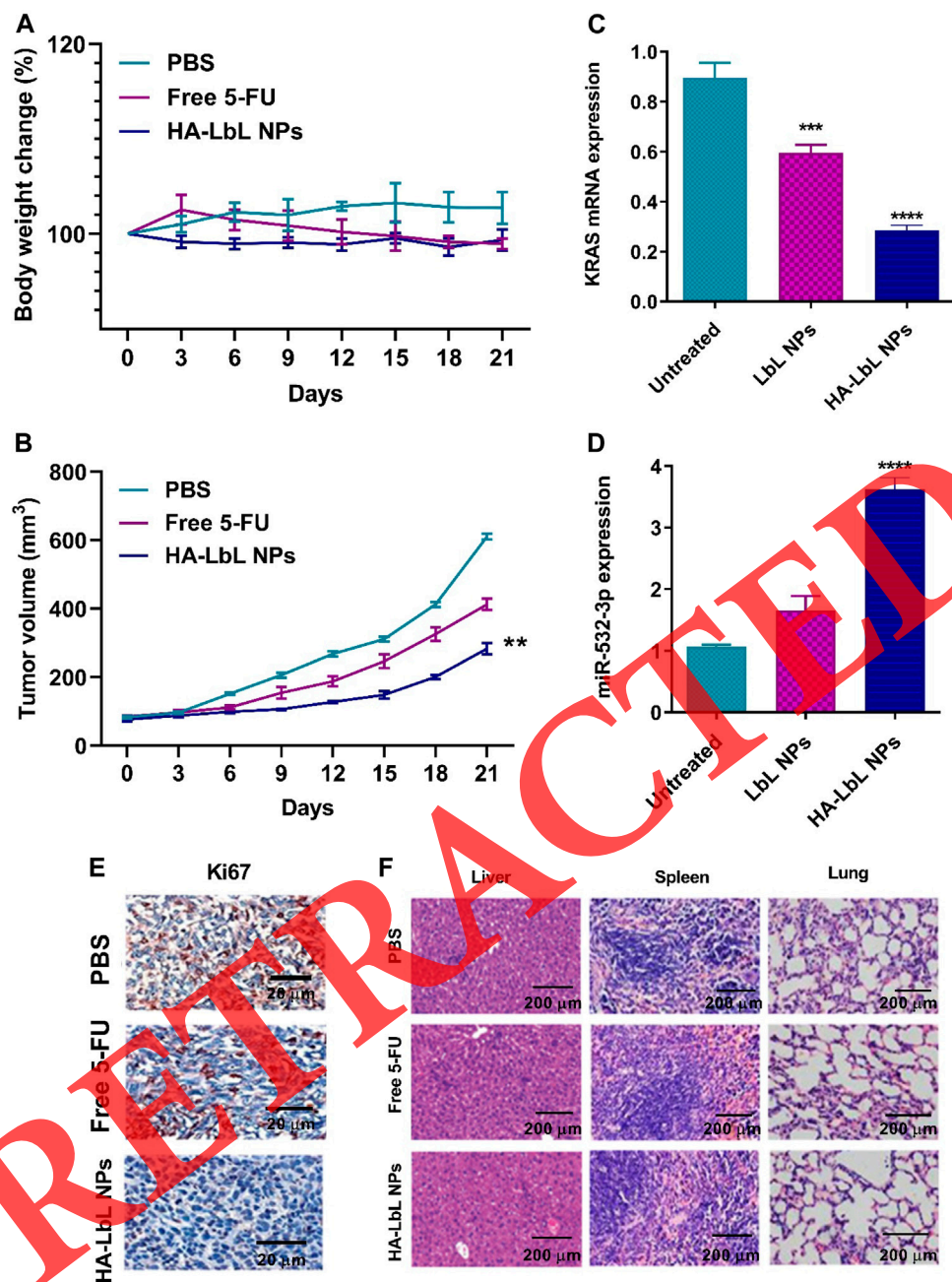
FIGURE 6
In vivo anti-tumor evaluation of LbL formulation in tumor-bearing mice after intravenous injection with PBS, free 5-FU, and HA-LbL NPs (*n* = 5/ each group). **(A)** Body weight curve; **(B)** Tumor volume curve. **(C)** Relative expression of KRAS; **(D)** Relative expression of miR-532-3p; **(E)** Immunostaining of Ki67; **(F)** H&E staining of liver, spleen, and lung. $**p < 0.01$, $***p < 0.01$, $****p < 0.01$.

hydration. Then, positively charged CS, negatively charged therapeutic RNAs (MiR-532-3p and si-KRAS), and positively charged CS were sequentially coated on the surface of the liposome. Finally, a negatively charged HA was adsorbed as the outermost layer due to its capability to target the CD44 receptor, an overexpressed receptor on the surface of CRC cells (Figure 1A). The TEM micrograph of liposomes displayed a uniform spherical structure with a diameter of around 95–100 nm (Figure 1B).

The particle size distribution and zeta potential of NPs are fundamental physical properties for maintaining their integrity and behaviors (Danaei et al., 2018). In this project, the successful

layer absorption on the liposome surface was affirmed by DLS, which demonstrated an approximately 10–15 nm increase in NPs diameter following the assembling of each layer (Figure 1C). The zeta potential characterization exhibited a charge inversion after assembling each layer (Figure 1D). In the next experiment, the PDI value of nanotherapeutics was similar and less than 0.2, indicating the narrow dispersity in the solution (Figure 1E). The stability tests exhibited only a slight growth (˂5%) in diameter size for LbL NPs in serum solution over time, suggesting the good stability of the presented nano-formulation (Figure 1F).

3.2 Encapsulation efficiency and drug release

In the prepared HA-LbL NPs, 5-FU as a hydrophilic drug was incorporated into the hydrophilic part of the liposomal vesicle. The EE% of 5-FU-loaded liposomes is an important feature for the effectiveness of the approach performed for encapsulation (Lollo et al., 2019). In the present study, the EE% of 5-FU-loaded liposomes was 62.12 ± 2.41%. The dialysis method assessed the carrier *in vitro* 5-FU release profile. *In vitro*, a 5-FU release investigation was performed in sterile PBS solution at pH 5.4, simulating the acidic lysosomal compartments and pH 7.4, simulating physiological conditions. As depicted in Figure 1G, we exhibited a slight release of 5-FU at pH 7.4 in PBS buffer (less than 50%) for 80 h. In contrast, 5-FU was released at about 80% at pH 4.5 during similar time points, indicating that 5-FU release from LbL NPs was both pHs- and time-dependent (Figure 1G). 5-FU released from HA-LbL NPs more sustainably reflected that HA-LbL NPs inhibited the drug release at the physiological pH and hindered the systemic drug toxicity.

3.3 Protection of miRNA/siRNA against RNase

The RNAs loaded on the HA-LbL NPs were in a 1:1 M ratio of miRNA to siRNA. The agarose gel electrophoresis was conducted under a 1:1 to 8:1 LbL NPs/RNAs ratio to determine the encapsulation efficiency of miRNA/siRNA into HA-LbL NPs. As demonstrated in Figure 1H, siRNA/miRNA could significantly bind to HA-LbL NPs over the ratio from 4:1 to 8:1, and no free RNAs were observed over a ratio of 4:1. This result indicated that LbL NPs could greatly bind to siRNA/miRNAs.

It has been well proven that RNAs such as miRNA and siRNA are quite unstable in serum due to degradation by serum nucleases, which is one of the main challenges in the systemic delivery of these molecules due to gene silencing (Lam et al., 2015). Therefore, it is very important to manufacture vehicles that could protect RNAs against the degradation by serum RNases. To demonstrate the role of HA-LbL NPs in

protecting siRNA/miRNA from serum RNases, the release of RNAs from HA-LbL NPs was investigated in serum. Agarose gel electrophoresis revealed that the RNAs incorporated in HA-LbL NPs were slightly released from the carrier after FBS incubation for 24 h, while free miRNA or free siRNA was rapidly degraded. These findings indicated the protection of RNAs by the HA-LbL NPs against degradation at pH 7.4 in FBS solution over an extended time (Figure 1I).

3.4 *In vitro* analysis

3.4.1 Cellular uptake and cytotoxicity of HA-grafted LbL NPs

Colorectal cancers have a high mutation frequency of KRAS and p53. Therefore, we have chosen a model of human colorectal cancer, SW480, known to present p53 ($^{R273H\ and\ P309S}$) and KRAS^{G12V}) mutations for further experiments (Spartalis et al., 2019). The nanoparticles' ability to internalize and accumulate in tumor cells strongly affects their therapeutic impacts (Duan and Li, 2013). In the current work, the inner core of the liposome was tagged with coumarin-6, and the uptake of HA-LbL NPs by SW480 cells was vitalized by the fluorescent images (Figure 2A). The fluorescence microscopy images showed that the ability of HA-tagged LbL NPs for trafficking across the SW480 cells was higher than LbL NPs without HA (Figure 2A). Mechanistically, the deposition of HA on the surface of LbL NPs could potentially increase this nanoparticle's therapeutic efficacy due to the tumor cells' high uptake ability. To confirm the effective entry of nanoparticles into the cell, we then measured miR-532-3p and KRAS expression by the q-RT-PCR technique. The data analysis indicated that the level of miR-532-3p highly increased, while KRAS expression was significantly suppressed after cell treatment with HA-LbL NPs group compared with LbL NPs and untreated groups (p˂0.01; Figures 2B,C).

To further investigate whether HA-LbL NPs affected the proliferation of CRC, we assessed the cell viability of cancer cells using an MTT assay. Figure 3 exhibited the viability of SW480 cells treated with blank LbL NPs, free 5-FU, LbL NPs, and HA-LbL NPs. As depicted in Figure 3A, blank LbL NPs did not display considerable cytotoxicity on SW480 cells, indicating the good biocompatibility of materials used to form these nano-size particles (Figure 3A). On the SW480 cell line, HA-LbL NPs exhibited remarkable cytotoxicity relative to free 5-FU and LbL NPs groups and untreated groups ($p < 0.01$; Figure 3B).

3.4.2 Invasion and migration assay

It is well proven that preventing cancer cell migration is an effective approach for CRC treatment by hindering tumor metastasis (van Noort et al., 2014). Previously, miR-532-3p was identified as one of the valuable tumor suppressor miRs downregulated in CRC. Gu

et al. described that miR-532-3p suppressed cell growth, migration, and EMT in HT29 cells (Gu et al., 2019). The present study revealed that HA-LbL NPs formulation containing miR-532-3p was successfully taken up by SW480 cells. In this experiment, we evaluated the ability of HA-LbL NPs to hinder SW480 cell migration and invasion by transwell chamber assay. Figures 4A,B indicate that untreated SW480 cells exhibited high migration and invasion capacity. Free 5-FU had little inhibition effect, whereas the migration and invasion of SW480 cells exposed to HA-LbL NPs were notably inhibited. These findings illustrated the synergistic effect of suppressing cancer cell migration and invasion through co-delivery of 5-FU and miR-532-3p by HA-LbL formulation. In the next experiment, the analysis of western blotting data revealed that the expression of MMP-2 and MMP-9 (two migration markers), as well as vimentin (mesenchymal marker), was significantly reduced, and the expression of E-cadherin (epithelial marker) was elevated after treatment of SW480 cells with HA-LbL NPs relative to free 5-FU and untreated cells (Figures 4C,D).

3.5 *In vivo* studies

3.5.1 Blood compatibility and immunogenicity of LbL NPs

Hemolysis rate and blood clotting indexes were measured to evaluate nanoparticle blood compatibility (Zook et al., 2011). As demonstrated in Figure 5A, the hemolysis rate of different concentrations of HA-LbL NPs was less than 6% after 4 and 24 h of incubation, which exhibited that these nano-formulations had no considerable deleterious effects on erythrocytes and did not result in hemolysis. Moreover, the analyses of blood clotting indexes also indicated that HA-LbL NPs had no significant effects on TT, PTT, PT, and fibrinogen (Figure 5B). These findings revealed that HA-LbL NPs did not affect the normal activity of the blood coagulation system. Altogether, these results suggested that HA-LbL NPs had good blood compatibility, an important characteristic for successful intravenous injection and systemic delivery.

3.5.2 *In vivo* biodistribution

To check the successful *in vivo* delivery of LbL NPs to the CRC tumor site, the biodistribution of LbL NPs was monitored in tumor-bearing mice using an *in-vivo* imaging system. As demonstrated in Figure 5C, after 2 h of intravenous injection with cy3-tagged HA-LbL NPs, the weak fluorescence signal was distributed in the tumor site. However, the fluorescence signals were mainly increased with elapsed time, revealing the accumulation of LbL NPs in the tumor site 6 h post intravenous injection.

3.5.3 *In vivo* anti-tumor efficacy

In vivo anti-tumor efficacy of HA-LbL NPs was examined on the tumor xenograft model, and body weight and tumor volume

curves are shown in Figures 6A,B. The mice were randomly divided into three groups to monitor the anti-tumor effects and then treated with saline as the control group, free 5-FU, and HA-LbL NPs, respectively. On day 21, mice treated with HA-LbL NPs illustrated no remarkable changes in body weight (Figure 6A), suggesting the good tolerance of this nano-system. As shown in Figure 6B, the HA-LbL NPs most efficiently reduced the tumor volume compared to free 5-FU and saline groups ($p < 0.01$). Compared to the saline and 5-FU groups, the HA-LbL NPs showed a better suppression impact on tumor growth ($p < 0.01$), which might be attributed to the efficient delivery of therapeutics to the tumor site by HA-LbL nanocarriers. Subsequently, q-RT-PCR analyses confirmed that HA-LbL NPs could efficiently deliver miRNA and siRNA to the tumor site. Most importantly, the successful target KRAS silencing was observed after HA-LbL NPs treatment ($p < 0.0001$; Figure 6C). As depicted in Figure 6D, the level of miR-532-3p was significantly elevated in the HA-LbL NPs group relative to other groups ($p < 0.0001$). Immunohistochemical staining in xenograft tumors also revealed lower proliferation marker Ki67 expression in the HA-LbL NPs group compared to the control group (Figure 6E). Finally, the *in vivo* safety of LbL NPs was assessed by H&E staining. As shown in Figure 6F, no considerable organ toxicity was visualized in the LbL NPs-treated group relative to the saline-treated group. The slight toxicity of LbL NPs may be attributed to their minimal retention in non-target tissues.

Conclusion

In conclusion, we have developed a strategy for the co-delivery of 5-FU, si-KRAS, and miRNA-532-3p using a layer-by-layer approach to treat CRC. This strategy revealed high uptake and significant tumor inhibition efficiency with no remarkable changes in body weight and organ toxicity. Compared to the free 5-FU formulation used alone, the co-delivery of the 5-FU and miRNA/siRNA greatly improved anti-tumor efficacy. This new nanoplatform is expected to be a good system with great potential for the synergetic treatment of CRC.

Data availability statement

The original contributions presented in the study are included in the article/supplementary material, further inquiries can be directed to the corresponding authors.

Ethics statement

The animal study was reviewed and approved by Shahid Sadoughi University (grant number: 12412).

Author contributions

MS, writing original draft. OA, graphics and pictures preparation. PD, *in vivo* experimental. BH, design and conceptualization, supervision, funding acquisition. FO, writing—reviewing and editing. DT, Editing.

Funding

Conflict of interest

The authors declare that the research was conducted in the absence of any commercial or financial relationships that could be construed as a potential conflict of interest.

Publisher's note

All claims expressed in this article are solely those of the authors and do not necessarily represent those of their affiliated organizations, or those of the publisher, the editors and the reviewers. Any product that may be evaluated in this article, or claim that may be made by its manufacturer, is not guaranteed or endorsed by the publisher.

References

Abtahi, N. A., Naghib, S. M., Ghalekohneh, S. J., Mohammadpour, Z., Nazari, H., Mosavi, S. M., et al. (2022). Multifunctional stimuli-responsive niosomal nanoparticles for co-delivery and co-administration of gene and bioactive compound: *In vitro* and *in vivo* studies. *Chem. Eng. J.* 429, 132090. doi:10.1016/j.cej.2021.132090

Blondy, S., David, V., Verdier, M., Mathonnet, M., Perraud, A., and Christou, N. (2020). 5-Fluorouracil resistance mechanisms in colorectal cancer: From classical pathways to promising processes. *Cancer Sci.* 111, 3142–3154. doi:10.1111/cas.14532

Boyiddle, C., Ruboyianes, M., Del Valle, E., Bubendorf, L., Trunzer, K., Pugh, J., et al. (2017). *Development of IHC staining protocols for assessment of PD-L1 expression in cytological samples*. United States: AACR.

Chen, Y., Gao, D.-Y., and Huang, L. (2015). *In vivo* delivery of miRNAs for cancer therapy: challenges and strategies. *Adv. drug Deliv. Rev.* 81, 128–141. doi:10.1016/j.addr.2014.05.009

Danaei, M., Dehghankhold, M., Ataei, S., Hasanzadeh Davarani, F., Javanmard, R., Dokhani, A., et al. (2018). Impact of particle size and polydispersity index on the clinical applications of lipidic nanocarrier systems. *Pharmaceutics* 10, 57. doi:10.3390/pharmaceutics10020057

Duan, X., and Li, Y. (2013). Physicochemical characteristics of nanoparticles affect circulation, biodistribution, cellular internalization, and trafficking. *Small* 9, 1521–1532. doi:10.1002/smll.201201390

Eygeris, Y., Patel, S., Jozic, A., and Sahay, G. (2020). Deconvoluting lipid nanoparticle structure for messenger RNA delivery. *Nano Lett.* 20, 4543–4549. doi:10.1021/acs.nanolett.0c01386

Gu, L., Deng, Z. J., Roy, S., and Hammond, P. T. (2017). A combination RNAi-chemotherapy layer-by-layer nanoparticle for systemic targeting of KRAS/P53 with cisplatin to treat non-small cell lung cancer. *Clin. Cancer Res.* 23, 7312–7323. doi:10.1158/1078-0432.ccr-16-2186

Gu, C., Cai, J., Xu, Z., Zhou, S., Ye, L., Yan, Q., et al. (2019). MiR-532-3p suppresses colorectal cancer progression by disrupting the ETS1/TGM2 axis-mediated Wnt/β-catenin signaling. *Cell Death Dis.* 10, 739–814. doi:10.1038/s41419-019-1962-x

Gupta, B., Ruttala, H. B., Poudel, B. K., Pathak, S., Regmi, S., Gautam, M., et al. (2018). Polyamino acid layer-by-layer (LbL) constructed silica-supported mesoporous titania nanocarriers for stimuli-responsive delivery of microRNA 708 and paclitaxel for combined chemotherapy. *ACS Appl. Mat. Interfaces* 10, 24392–24405. doi:10.1021/acsami.8b06642

Huang, D., Sun, W., Zhou, Y., Li, P., Chen, F., Chen, H., et al. (2018). Mutations of key driver genes in colorectal cancer progression and metastasis. *Cancer Metastasis Rev.* 37, 173–187. doi:10.1007/s10555-017-9726-5

Keum, N., and Giovannucci, E. (2019). Global burden of colorectal cancer: emerging trends, risk factors and prevention strategies. *Nat. Rev. Gastroenterol. Hepatol.* 16, 713–732. doi:10.1038/s41575-019-0189-8

Lam, J. K., Chow, M. Y., Zhang, Y., and Leung, S. W. (2015). siRNA versus miRNA as therapeutics for gene silencing. *Mol. Ther. - Nucleic Acids* 4, e252. doi:10.1038/mtna.2015.23

Lollo, G., Matha, K., Bocchiardo, M., Bejaud, J., Marigo, I., Virgone-Carlotta, A., et al. (2019). Drug delivery to tumours using a novel 5-FU derivative encapsulated into lipid nanocapsules. *J. drug Target.* 27, 634–645. doi:10.1080/1061186x.2018.1547733

Lu, T. X., and Rothenberg, M. E. (2018). MicroRNA. *J. allergy Clin. Immunol.* 141, 1202–1207. doi:10.1016/j.jaci.2017.08.034

Meerloo, J. V., Kaspers, G. J., and Cloos, J. (2011). *Cell sensitivity assays: the MTT assay, cancer cell culture*. Germany: Springer, 237–245.

Men, W., Zhu, P., Dong, S., Liu, W., Zhou, K., Bai, Y., et al. (2020). Layer-by-layer pH-sensitive nanoparticles for drug delivery and controlled release with improved therapeutic efficacy *in vivo*. *Drug Deliv.* 27, 180–190. doi:10.1080/10717544.2019.1709922

Mirhosseini, M., Shekari-Far, A., Hakimian, F., Haghiralsadat, B. F., Fatemi, S. K., and Dashtestani, F. (2020). Core-shell Au@ Co-Fe hybrid nanoparticles as peroxidase mimetic nanozyme for antibacterial application. *Process Biochem.* 95, 131–138. doi:10.1016/j.procbio.2020.05.003

Nakayama, M., and Oshima, M. (2019). Mutant p53 in colon cancer. *J. Mol. Cell Biol.* 11, 267–276. doi:10.1093/jmcb/mjy075

Oroojalian, F., Rezayan, A. H., Shier, W. T., Abnous, K., and Ramezani, M. (2017). Megalin-targeted enhanced transfection efficiency in cultured human HK-2 renal tubular proximal cells using aminoglycoside-carboxyalkyl-polyethylenimine-containing nanoplexes. *Int. J. Pharm.* 523, 102–120. doi:10.1016/j.ijpharm.2017.03.024

Porru, M., Pompili, L., Caruso, C., Biroccio, A., and Leonetti, C. (2018). Targeting KRAS in metastatic colorectal cancer: current strategies and emerging opportunities. *J. Exp. Clin. Cancer Res.* 37, 57–10. doi:10.1186/s13046-018-0719-1

Pourpirali, R., Mahmoudnezhad, A., Oroojalian, F., Zarghami, N., and Pilehvar, Y. (2021). Prolonged proliferation and delayed senescence of the adipose-derived stem cells grown on the electrospun composite nanofiber co-encapsulated with TiO2 nanoparticles and metformin-loaded mesoporous silica nanoparticles. *Int. J. Pharm.* 604, 120733. doi:10.1016/j.ijpharm.2021.120733

Spartalis, C., Schmidt, E. M., Elmasry, M., Schulz, G., Kirchner, T., and Horst, D. (2019). *In vivo* effects of chemotherapy on oncogenic pathways in colorectal cancer. *Cancer Sci.* 110, 2529–2539. doi:10.1111/cas.14077

Strand, M. S., Krasnick, B. A., Pan, H., Zhang, X., Bi, Y., Brooks, C., et al. (2019). Precision delivery of RAS-inhibiting siRNA to KRAS driven cancer via peptide-based nanoparticles. *Oncotarget* 10, 4761–4775. doi:10.18632/oncotarget.27109

Sung, H., Ferlay, J., Siegel, R. L., Laversanne, M., Soerjomataram, I., Jemal, A., et al. (2021). Global cancer statistics 2020: GLOBOCAN estimates of incidence and mortality worldwide for 36 cancers in 185 countries. *Ca. A Cancer J. Clin.* 71, 209–249. doi:10.3322/caac.21660

van Noort, V., Schölch, S., Iskar, M., Zeller, G., Ostertag, K., Schweitzer, C., et al. (2014). Novel drug candidates for the treatment of metastatic colorectal cancer through global inverse gene-expression profiling. *Cancer Res.* 74, 5690–5699. doi:10.1158/0008-5472.can-13-3540

Vodenkova, S., Buchler, T., Cervena, K., Veskrnova, V., Vodicka, P., and Vymetalkova, V. (2020). 5-fluorouracil and other fluoropyrimidines in colorectal cancer: Past, present and future. *Pharmacol. Ther.* 206, 107447. doi:10.1016/j.pharmthera.2019.107447

Xie, Y., Wang, Y., Li, J., Hang, Y., Jaramillo, L., Wehrkamp, C. J., et al. (2018). Cholangiocarcinoma therapy with nanoparticles that combine downregulation of

MicroRNA-210 with inhibition of cancer cell invasiveness. *Theranostics* 8, 4305–4320. doi:10.7150/thno.26506

Xie, Y.-H., Chen, Y.-X., and Fang, J.-Y. (2020). Comprehensive review of targeted therapy for colorectal cancer. *Signal Transduct. Target. Ther.* 5, 22–30. doi:10.1038/s41392-020-0116-z

Ye, J., Lin, M., Zhang, C., Zhu, X., Li, S., Liu, H., et al. (2020). Tissue gene mutation profiles in patients with colorectal cancer and their clinical implications. *Biomed. Rep.* 13, 43–48. doi:10.3892/br.2020.1303

Yu, Q., Xiong, X., Zhao, L., Xu, T., and Wang, Q. (2020). Antifibrotic effects of specific siRNA targeting connective tissue growth factor delivered by polyethyleneimine-functionalized magnetic iron oxide nanoparticles on LX-2 cells. *Mol. Med. Rep.* 21, 181–190. doi:10.3892/mmr.2019.10834

Zhang, Y., Xiong, G. M., Ali, Y., Boehm, B. O., Huang, Y. Y., and Venkatraman, S. (2021). Layer-by-layer coated nanoliposomes for oral delivery of insulin. *Nanoscale* 13, 776–789. doi:10.1039/d0nr06104b

Zhao, Y.-C., Zhang, L., Feng, S.-S., Hong, L., Zheng, H.-L., Chen, L.-L., et al. (2016). Efficient delivery of Notch1 siRNA to SKOV3 cells by cationic cholesterol derivative-based liposome. *Int. J. Nanomedicine* 11, 5485–5496. doi:10.2147/ijn.s115367

Zhao, J., Wan, Z., Zhou, C., Yang, Q., Dong, J., Song, X., et al. (2018). Hyaluronic acid layer-by-layer (LbL) nanoparticles for synergistic chemo-phototherapy. *Pharm. Res.* 35, 196–214. doi:10.1007/s11095-018-2480-8

Zook, J. M., MacCuspie, R. I., Locascio, L. E., Halter, M. D., and Elliott, J. T. (2011). Stable nanoparticle aggregates/agglomerates of different sizes and the effect of their size on hemolytic cytotoxicity. *Nanotoxicology* 5, 517–530. doi:10.3109/17435390.2010.536615